Approach to standardize a spray-flame nanoparticle synthesis burner

J. Menser[*,1], S. Kluge[1], H. Wiggers[1,2], T. Dreier[1,2], C. Schulz[1,2]

[1]IVG, Institute for Combustion and Gas Dynamics – Reactive Fluids, University of Duisburg-Essen, Germany
[2]CENIDE, Center for Nanointegration Duisburg-Essen, Duisburg, Germany

Abstract

In this work, a standard burner for spray-flame nanoparticle synthesis is suggested. This device features an easy usability, high modularity and facilitates optical diagnostics and computational fluid dynamics compared to previous geometries. Main differences to other burners are a premixed flat flame for flame stabilization and a fully adjustable liquid fuel inlet. Preliminary characterizations of the spray and the synthesized particles are shown.

Introduction

Standard burners have been developed in the past for investigating laminar sooting flames [1-2] both as a validation tool in modeling soot chemistry and for developing optical soot diagnostics methods. Also for non-sooting turbulent flames, standardization has been used for a long time to advance both measurement technology and simulation through direct interaction. A few burner concepts for nanoparticle synthesis are frequently used in several labs and are commercially available, but they are not well suited for fundamental studies because their geometry is neither ideal for *in situ* measurements (e.g., particle sizing with LII or gas-phase temperature imaging via LIF), nor easy to simulate because they require extreme grid resolution.

Spray-flame synthesis is frequently used for generating metal oxide and ceramic nanoparticles [3]. Many precursors for nanoparticle synthesis (such as metal acetylacetonates, carbonates or nitrates) can be dissolved in alcohols or aromatic hydrocarbons (e.g., isopropanol and toluene). Therefore, low-cost precursors can be introduced in relatively high concentration into the flame together with the liquid fuel to produce sizable amounts of particulates for further processing.

This work focuses on the development and characterization of a standardized burner for spray-flame synthesis of nanoparticles. The main objectives are an optimization for computational fluid dynamics, a high modularity and an easy-to-assemble device.

Burner design

Fig. 1 shows an exploded view of the disassembled burner. In this burner a small diameter tube (a) delivers the liquid fuel/precursor solution. To guarantee a fit to the upper edge of the nozzle the tube can be drilled in and out by a fine pitch screw (b). Three micrometer screws (c) enable the adjustment of the position of the tube to optimize burning conditions during operation.

An annular slit surrounds the innermost tube for the liquid inlet. Through this nozzle the oxidizer is injected and helps vaporizing the liquid. The velocity of the oxidizer flow is about 100 m/s.

Both nozzles are located in the center of a large brass sinter plate (e) (mean porosity of 60 µm) simultaneously supporting a premixed pilot flame (0.5 standard liter per minute (slm) methane and 1.2 slm oxygen) and a co-flow of nitrogen or air. The respective flows to the burner are controlled by mass flow controllers (Bronkhorst) which are connected to a National Instruments Compact FieldPoint system. This system provides analog voltage signals to set and read-out the respective mass flow controllers. These flows are internally separated by a short tube section (d). To provide a preferably laminar gas flow the two gas flows are adjusted to generate the same cold gas velocity by scaling with the respective area of the ring segment. By varying the tube diameter of the separator a big range of flow rates for the pilot flame can be used changing also the enthalpy provided to the system by the primary flame.

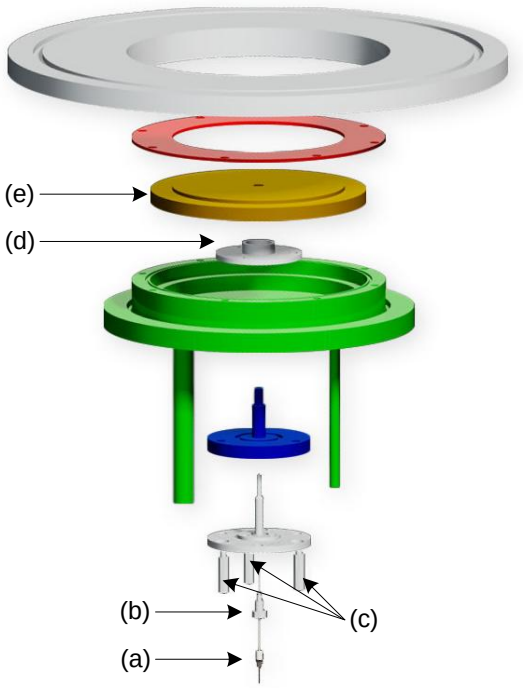

Fig. 1: Exploded view of the burner.

[*] Corresponding author: jan.menser@uni-due.de

The size and degree of agglomeration of nanoparticles strongly depends on the process pressure [4]. Therefore it is of interest to operate the burner under variable pressure conditions. The suggested burner can be easily adapted to vacuum chambers and filter systems by standardized ISO-K flanges. The coflow generated by the large diameter of the sintered matrix decouples the reaction zone from the wall. This significantly facilitates the simulation, which might otherwise need to consider perturbations through heat transfer. In addition, the particle deposition on walls and windows is minimized.

In the current setup a flow of 0.5 slm methane and 1.2 slm O_2 is provided for the pilot flame which then contributes 300 W of thermal power. This construction generates a blurred transition region between the flame-stabilizing co-flow and the pilot-flame which enables computational fluid dynamics simulations with moderate mesh size in regions that are not relevant for the process of interest, i.e. the synthesis flame and exhaust region. The sintered matrix design also guarantees a reproducible geometry without complex alignment.

Spray characterization

Spray break-up was characterized with a three-color shadowgraph method. The volume of interest was illuminated by red/green/blue light emitting diodes (LED) triggered with a temporal delay of 20 µs and an illumination time for each color of 3 µs. A consumer digital single-lens reflex (DSLR) camera with a red/green/blue color sensor collected the stray light induced by the droplets. The droplets were imaged with a magnification of 2:1 onto the CCD detector with a pixel size of 7×7 µm^2, and were sized and counted in post-processing steps.

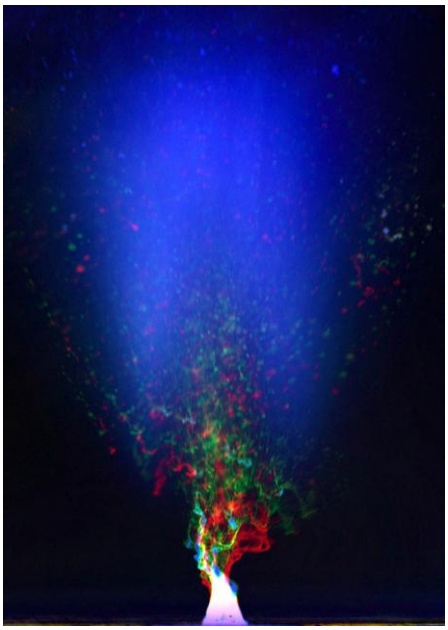

Fig. 2: Photograph of droplets illuminated with red/green/blue LEDs in a burning spray flame. Due to the bluish chemiluminescence of the ethanol flame the blue channel is not used in further data evaluation steps.

By separating each color of the picture with image processing the time-steps are recovered. The velocity profile was calculated with the open source toolbox PTVLab [5] for Matlab. The power of the LEDs was sufficient to obtain good quality particle images with even a burning flame (Fig. 2).

Fig. 3 shows the droplet velocity as a function of height above burner (HAB). The liquid fuel/precursor solution was injected through the capillary with 1 m/s and starts vaporizing in the surrounding gas stream. The droplets are simultaneously accelerated to about 40 m/s. The liquid break-up at about 1 to 2 mm above the nozzle exit reveals an oscillation of the filaments from side to side [6]. These filaments break up into droplets and discontinuously provide spray droplets.

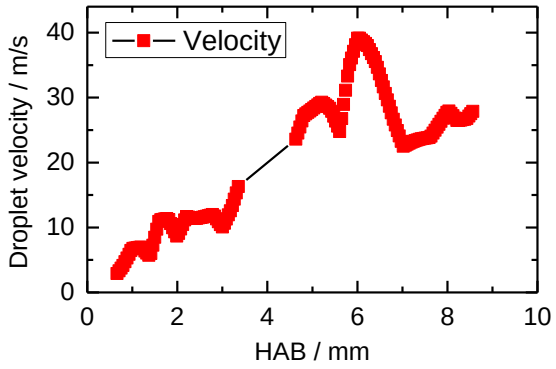

Fig. 3: Velocity of the droplets depending on HAB.

The break-up of large ligaments forms droplets with a particle size-distribution shown in Fig. 4. The droplet-size distribution has a maximum at about 100 µm with a not negligible number of particles larger than 200 µm.

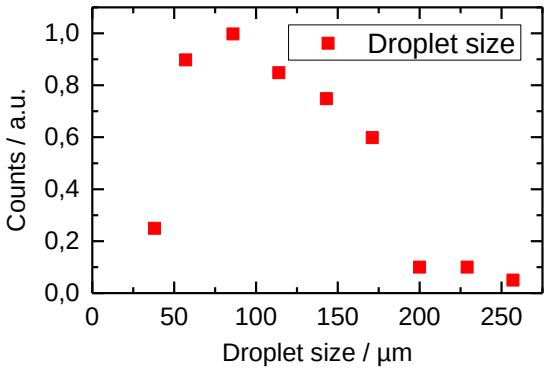

Fig. 4: Droplet size-distribution of the spray.

Burner operation under synthesis conditions

The burner was tested under synthesis conditions (i.e., with precursor addition) while simultaneously applying optical diagnostics. For producing nanoparticles in sizable amounts, synthesis may take hours of operation during which the sintered matrix is exposed to precursor chemicals, intermediates and product particles. Especially unburned precursors penetrating the matrix material could be problematic. Due to thermal decomposition of the precursor solid matter can be

formed inside the matrix pores and plugs the gas flow. This can lead to instability of the pilot flame and the sheath gas-flow. Closer inspection revealed that even after 20 hours of operation the matrix was not contaminated with nanoparticles (Fig. 7).

The mean temperature of the matrix can be estimated using temper colors [7]. The top side of the brass matrix turned black directly during the first use of the matrix. Here, temperatures above 300°C have been reached. It is not possible to specify an upper temperature limit, because black already states the maximum assignable temperature with temper colors. On the bottom side the temperature reaches 300°C (dark-gray coloring of the brass) right below the pilot flame. The FKM O-ring seal separating sheath gas and pilot flame flow has a maximum operation temperature of 220°C but is still ready for use. Outside the O-ring seal the color changes from dark-gray to orange-grey (270°C), blue (240°C) and darker-bronze (180°C) within 1 cm. It needs to be noted that temperatures determined using temper colors are just rough estimates. The color depends on annealing time and gas composition.

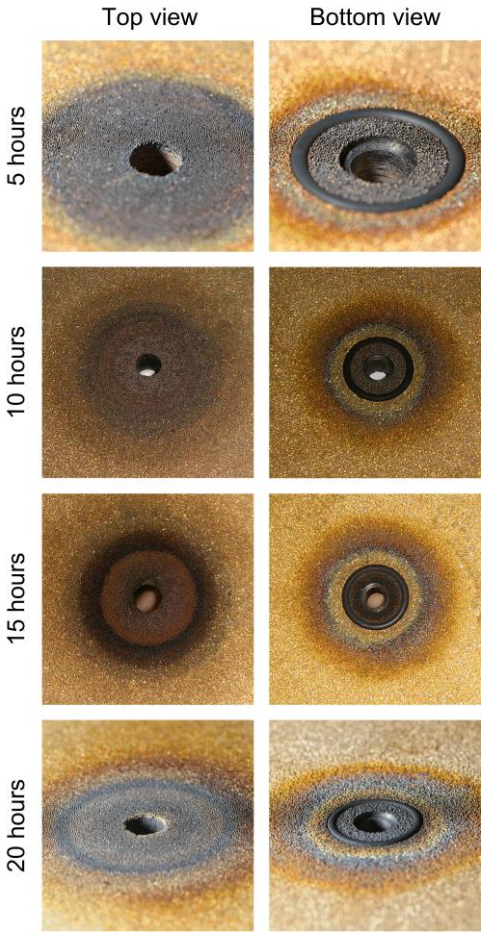

Fig. 5: Temper colors of the sintered matrix over a time period of 20 hours. The sintered matrix reaches temperatures of 300°C.

Comparison of nanomaterials synthesized with different spray nozzles

For the synthesis of nanoparticles as basic component for battery anode and cathode materials several spray flame processes have been used, mainly for the titania and manganese-silicate synthesis. Here, these materials were characterized with optical microscopy and spontaneous Raman spectroscopy to characterize morphology and composition.

Especially for titania and silica, the Raman shift includes information about mean particle size [8-9]. Fig. 6a shows a comparison of the nanomaterials formed from the same precursors using as similar as possible synthesis conditions with the new spray-flame burner and an established burner [10]. The main differences are the design of the pilot flame inlet (annular gap to flat flame) and the amount of sheath gas.

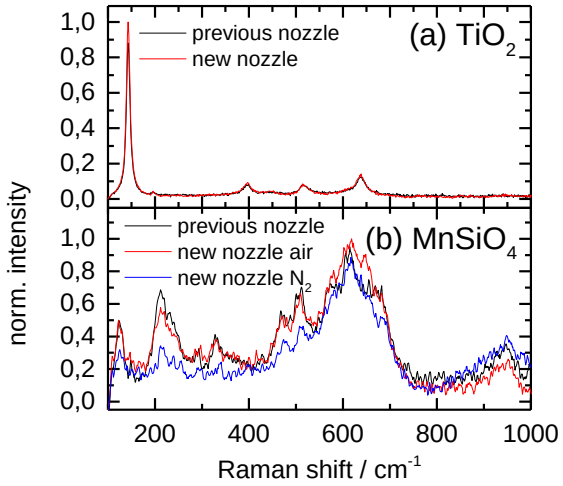

Fig. 6: Raman spectra of titania and manganese-silicates.

The spectra of TiO_2 (Fig. 6a) show no significant deviations. The titania phase presumably is Anatase (peaks at 142, 396, 516, and 639 cm^{-1}), only a small contamination with the Rutile phase (peaks at 540 and 615 cm^{-1}) was observed. Exploiting the phonon confinement effect the median size of the particle size distribution was estimated to about 12 nm. To confirm the equality of both particle syntheses further comparisons with TEM and XRD need to be done.

Fig. 6b shows Raman spectra of manganese silicates generated with the previous and the new burner with different sheath gases (compressed air and nitrogen). The interpretation of the spectra of manganese silicates is more complex. Until now, publications about Raman and diffraction-based measurements of $MnSiO_4$ are rare. The spectra show contributions of MnO_2 [11], Mn_3O_4 [12], SiO_2 [13], and additional peaks at 120 and 220 cm^{-1} that cannot be assigned to a particular crystal phase. It can be assumed that in addition to $MnSiO_4$ other phases are present. This shows that the burner geometry has far less influence on the crystal structure than the sheath gas composition.

Optical microscopy revealed a change in spectral emission characteristics (Fig. 7). While the material synthesized with the previous nozzle is light grey with brownish surfaces, this nozzle produces darker particles with white and lucid spots. The fact, that the Raman spectra show a distinct SiO_2 phase may be due to the presence of extended silicate crystals.

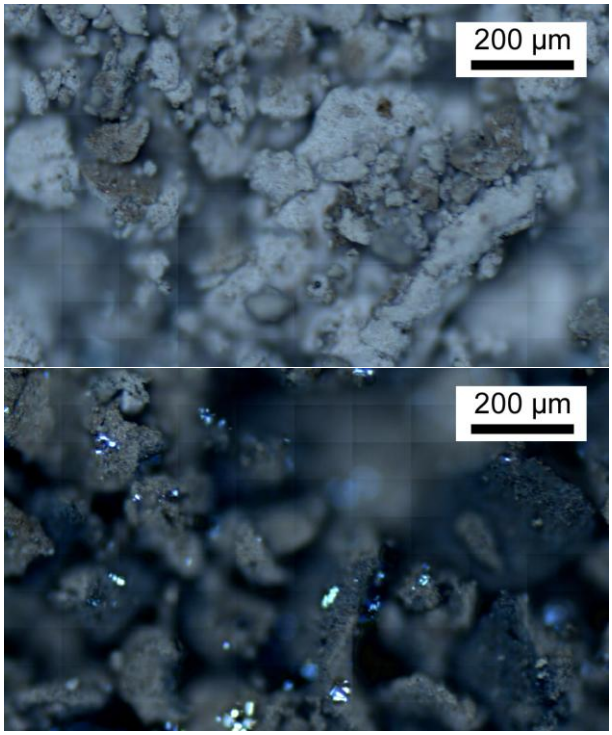

Fig. 7: Stitched microscopic images of manganese silicate synthesized with the previous (upper image) and new burner (lower image). This image shows a change of the optical properties and crystallinity.

Conclusions

In this work we present an easy to construct and fabricate nozzle-type burner for flame-based nanoparticle synthesis. It consists of a central nozzle, a concentric pilot flame and a large diameter coflow. This setup improves the previous concepts and offers following advantages:

- The pilot flames is symmetrical and does not require any adjustment
- The capillary tube is fully adjustable with three micrometer screws even within the running experiment
- The burner can be adapted to various conditions, especially optical diagnostics
- The large sintered matrix causes a laminar surrounding gas stream and therefore makes it easier to implement into suitable CFD-modeling approaches

Acknowledgements

The authors acknowledge technical support by J. Kovacevic. This work was funded by the German Research Foundation (DFG) within SCHU 1369/14.

References

[1] R. Santoro, H. Semerjian, R. Dobbins, Combust. Flame 51 (1983) 203-218.
[2] D. R. Snelling, K. A. Thomson, G. J. Smallwood, Ö. L. Gülder, Appl. Opt. 38 (1999) 2478-2485.
[3] S. E. Pratsinis, Prog. Energy Combust. Sci. 24 (1998) 197-219.
[4] S. Hardt, A. Hamid, C. Weise, I. Wlokas, H. Wiggers, C. Schulz, Proceedings of the 2011 AIChE Annual Meeting Conference (2011) 16-21.
[5] W. Brevis, Y. Niño, G. H. Jirka, Exp. Fluids 50 (2011) 135-147.
[6] C. Weise, J. Menser, S. A. Kaiser, A. Kempf, I. Wlokas, Proc. Combust. Inst. 35 (2015) 2259-2266.
[7] P. Gordon, J. Heat Treating 1 (1979) 93-93.
[8] D. Georgescu, L. Baia, O. Ersen, M. Baia, S. Simon, J. Raman Spectrosc. 43 (2012) 876-883.
[9] C. Meier, S. Lüttjohann, V. G. Kravets, H. Nienhaus, A. Lorke, H. Wiggers, Physica E 32 (2006) 155-158.
[10] L. Mädler, H. K. Kammler, R. Mueller, S. E. Pratsinis, J. Aerosol Sci. 33 (2002) 369-389.
[11] S. Cheng, L. Yang, D. Chen, X. Ji, Z.-j. Jiang, D. Ding, M. Liu, Nano Energy 9 (2014) 161-167.
[12] J. Zuo, C. Xu, Y. Liu, Y. Qian, Nanostruct. Mater. 10 (1998) 1331-1335.
[13] T. Sato, N. Funamori, T. Yagi, Nat. Commun. 2 (2011) 345.